IEEE Photonics Journal
An IEEE Photonics Society Publication

Open Access

S-Band Gain Improvement Using a Thulium–Aluminum Co-Doped Photonic Crystal Fiber Amplifier

Volume 6, Number 6, December 2014

S. D. Emami
A. R. Muhammad
S. Z. Muhamad-Yasin
K. A. Mat-Sharif
M. I. Zulkifli
F. R. M. Adikan
H. Ahmad
H. A. Abdul-Rashid

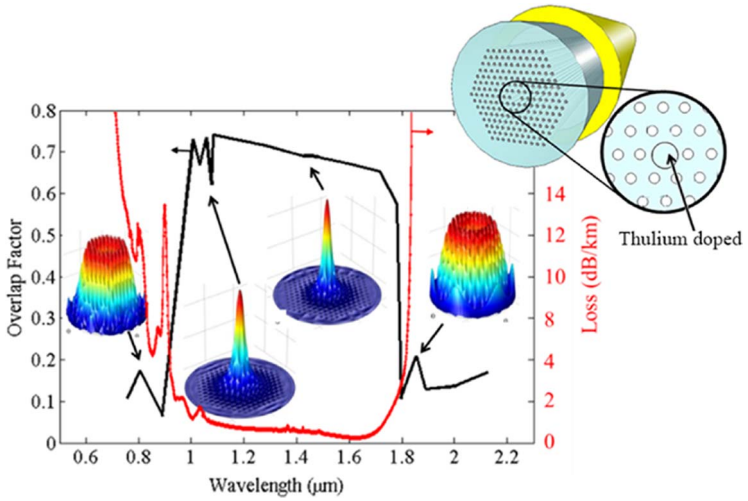

DOI: 10.1109/JPHOT.2014.2366158
1943-0655

S-Band Gain Improvement Using a Thulium–Aluminum Co-Doped Photonic Crystal Fiber Amplifier

S. D. Emami,[1] A. R. Muhammad,[2] S. Z. Muhamad-Yasin,[1] K. A. Mat-Sharif,[1] M. I. Zulkifli,[1] F. R. M. Adikan,[3] H. Ahmad,[2] and H. A. Abdul-Rashid[1]

[1]Faculty of Engineering, Multimedia University, 63100 Cyberjaya, Malaysia
[2]Photonic Research Center, Physics Department, University of Malaya, 50603 Kuala Lumpur, Malaysia
[3]Department of Electrical Engineering, University Malaya, 50603 Kuala Lumpur, Malaysia

DOI: 10.1109/JPHOT.2014.2366158

Manuscript received August 25, 2014; revised October 16, 2014; accepted October 25, 2014; date of current version November 20, 2014. This work was supported by Telekom Malaysia through its research funding program under Grant RDTC 110766. Corresponding author: S. D. Emami (e-mail: s.d.emami@gmail.com).

Abstract: An extended method for gain and noise figure enhancement in the S-band using a thulium-doped photonic crystal fiber amplifier (TD-PCFA) is proposed and shown by numerical simulation. The principle behind the enhancement is the suppression of unwanted amplified spontaneous emission (ASE) using the PCF structure. This proposed PCF achieves the intended band-pass by doping the cladding with high index material and realizes appropriate short and long cut-off wavelengths by enlarging the air-holes surrounding the doped core region. The PCF geometrical structure is optimized so that high losses occur below the short cut-off wavelength (800 nm) and beyond the long cut-off wavelength (1750 nm). Furthermore, the PCF geometrical structure design allows for high ASE suppression at 800- and 1800-nm band, thus increasing the population inversion needed for amplification in S-band region as the 1050-nm pump propagates light in the band-pass. The proposed TD-PCFA demonstrates gain enhancements of 3–6 dB between 1420 and 1470 nm.

Index Terms: Optical fiber amplifier, TDFA, PCF, ASE suppression.

1. Introduction

Optical amplifiers have proven essential to fulfilling increasing Internet traffic demands in recent years. Projected demands mean that broadband optical amplifiers must be able to amplify the new short wavelength band (S-band) in addition to the existing C- and L-bands. Thulium-doped fiber amplifiers (TDFAs) are a promising candidate for S-band amplification since the amplification bandwidth of the TDFA is centered at 1470 nm [1].

Experimental and numerical studies have been made on multi-component silica hosts such as aluminum in order to reduce phonon energy that disrupts amplification [2]–[4]. Gain improvement in the S-band region can occur by suppressing the amplified spontaneous emission (ASE) at the 800 nm and 1800 nm bands [5]. Various methods proposed for filtering out unwanted ASE on doped fiber include long-period fiber gratings, bend-loss and band-gap filtering [5]–[8]. One of the most effective methods of suppression of both 800 nm and 1800 nm bands, is shown experimentally and numerically using macro-bending approach on silica based TDF [5]. The

macro-bending technique involves bending a fiber in excess of a certain threshold radius, which results in the fiber having a suppressing effect on unwanted emission [6]. High attenuation due to higher order mode loss occurs below 1000 nm cut-off wavelength, and loss due to bending increases with longer wavelengths. An effective design enhancing both of these losses exploits a larger mode field diameter (MFD) that suppresses 800 nm and 1800 nm bands respectively, resulting in higher stimulated emission and better S-band amplification [5].

Recently, photonic crystal fiber (PCF) has been reported as an alternative ASE suppression method [9]. In a related development, a thulium-doped PCF fabrication with the aim of filtering ASE above 1900 nm resulted in a downshift gain towards the L-band wavelength region [10]. Another proposed design [7] for S-band amplification using erbium has the possibility of a design variation whereby PCF is included in order to reduce the overlap factor for a particular wavelength range.

This current work extends the reported ASE suppression method using PCF [7], [9]–[11] with the aim of suppressing ASE in the TDF to achieve a superior S-band gain. The proposed design [11] demonstrates that the optimized PCF geometrical structure results in short and long cut-off wavelengths to achieve desired filtering characteristics. In order to achieve a low pass filter effect around 1.7 μm, the first layer of air holes requires a larger diameter to provide low confinement loss at short wavelengths. The fabrication of the proposed PCF filter was published in [10]. It is shown that by increasing the wavelength, the electric field gradually crosses the layer increasing loss near 1.9 μm. Confinement losses of 3.3×10^{-8} dB/m and 6.7×10^{-5} dB/m are measured at 1.7 μm and 1.9 μm, respectively

Numerical modeling results of a distributed optical band-pass filter to suppress 800 nm and 1800 nm unwanted ASE using a thulium–aluminum co-doped photonic crystal fiber are reported in this paper. The proposed PCF band-pass short and long cut-off wavelengths are achieved by doping the fiber cladding with high index material and enlarging the air-holes surrounding the doped core region [11]. The transmission characteristics are verified via full-vectorial finite-element method (FV-FEM). Subsequently, the thulium-doped photonic crystal fiber amplifier (TD-PCFA) overlap factor is investigated. Minimal loss and high overlap factors for S-band signal are observed in the optimized TD-PCFA. Higher loss and low overlap factors are determined for 800 nm and 1800 nm ASE, corresponding to gain and noise figure improvements of 5 dB and 1 dB, respectively [12]. The fabrication tolerance for the TD-PCFA is also presented for practical consideration.

2. Operating Principles of Thulium–Aluminum CO-Doped PCF Amplifier (TD-PCFA)

2.1. PCF Band-Pass Filter

PCF with differing structures can possess dissimilar characteristics, especially in their transmission windows or band-pass region [9], [13]–[15]. One impressive band-pass filter was developed based on index-guiding, solid-core, and single-mode PCF [11]. In the band-pass filter proposed here, the short cut-off wavelength is achieved by the difference of core and clad refractive index for particular materials, while the long- cut-off wavelength is obtained by manipulating the size of air-holes in the first ring surrounding the central core. Fig. 1(a) represents a cross-section view of the proposed PCF band-pass filter. Four important geometrical properties to characterize this PCF are lattice constant Λ, core diameter D $(\Lambda = D)$, diameter d' of the first ring of air-holes surrounding the core, and outer ring air-holes diameter d. This PCF was modeled with a solid core waveguide that exploits total internal reflection (TIR) principles instead of those of photonic band-gap in hollow core PCF. The total internal reflection is caused by the lower effective index in the microstructured air-filled region. [13]. It is crucial to distinguish the diameter size between d' and d, since this aspect affects the cut-off wavelengths of the band-pass filter. The other important parameter of this proposed PCF is core-cladding refractive index

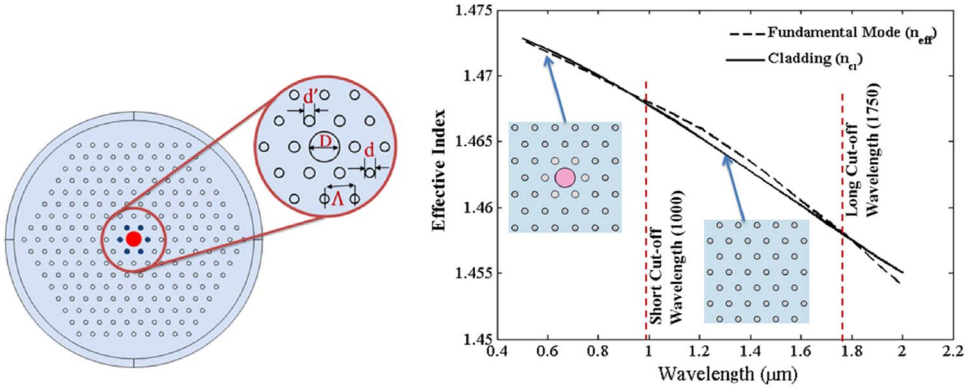

Fig. 1. Geometrical structure of PCF (cross-section view). (b) Fundamental mode and cladding effective refractive index variation for a PCF with $d'/\Lambda = 0.35$, $d/\Lambda = 0.30$, and $\Delta = -0.004$.

difference ($\Delta = n_{core} - n_{cladding}$). Tailoring the refractive index of aluminum-doped silica fiber can be realized by using different concentration of Al_2O_3 [16].

In this model, the short and long cut-off wavelengths of PCF are dependent on the intersection point of effective refractive index of fundamental mode with effective refractive index of cladding mode. Fig. 1(b) shows the fundamental mode refractive index and cladding refractive index as a function of wavelength. The PCF structural parameters are set at $d'/\Lambda = 0.35$, $d/\Lambda = 0.30$, $\Delta = -0.004$ and at fixed pitch constant $\Lambda = 3.2$ μm. Short cut-off wavelength λ_S can be obtained when the effective refractive index of fundamental mode lines intersects with the cladding index at low wavelength. Beyond λ_S, the mode field is well-confined in the central core due to the higher effective refractive index of core in comparison to the cladding. The relation of the first air-holes ring diameter size to the core effective refractive index becomes apparent when the size is smaller than the effective cladding refractive index n_{eff} at a certain wavelength. The n_{eff} also intersects with $n_{cladding}$ beyond 1600 nm, and this feature is called the long cut-off wavelength λ_L. Hence, the transmission windows are determined within the region between λ_S and λ_L.

Fabrication is possible by means of the classical stack and draw method [10]. Different capillary sizes of first layer and following seven layers are stacked hexagonally around a central thulium-doped silica rod fabricated by the MCVD process associated with the solution doping technique. The PCF preform is subsequently drawn into a PCF fiber using a drawing tower while an intra-air-holes over-pressure is applied in order to control the air-hole dimensions [10]

2.2. Optimization for ASE Suppression

Earlier reports show an enhancement of TDFA performance by suppressing the ASE at both 800 nm and 1800 nm [5]. The introduced PCF filter functions as a distributed filter to suppress the ASE simultaneously at 800 nm and 1800 nm bands. Achieving the desired band-pass filtering requires optimization of the PCF physical dimensions. The objective of this optimization is to suppress the ASE by the following criteria:

a) The pump at 1050 nm must be propagating with low loss and high overlap factors.
b) The 1460 nm signals must be propagating with low loss and high overlap factors.
c) The 800 nm ASE has to be propagating with high loss and low overlap factors, with the range of short cut-off wavelength between 900–1000 nm.
d) The 1800 nm ASE has to be propagating with high loss and low overlap factors, with the range of long cut-off wavelength between 1600–1700 nm.

Fulfilling the design criteria necessitates consideration of a variety of PCF design parameters. A transmission window can be made narrow by utilization of a high core-cladding index contrast

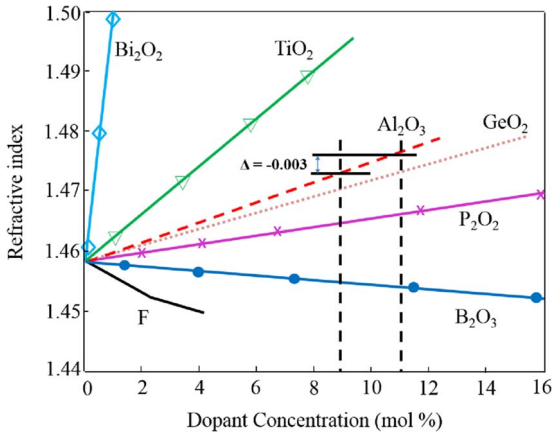

Fig. 2. Refractive index as a function of dopant concentration for Bi_2O_3, iO_2, Al_2O_2, GeO_2, P_2O_2, B_2O_3, and F.

and a large first ring air-holes diameter. Conversely, using a low core-cladding index contrast together with a small first ring air-holes diameter corresponds to a broader transmission window [11]. Fig. 2 shows the variation of refractive index versus dopant concentration for different materials such as Al_2O_2, GeO_2, and F [16]. A core-cladding doping concentration difference Δ can be achieved by co-doping with different concentrations (mol%) of different materials. Co-doping with heavy metal oxides such as Al_2O_3 is reported to increase the Tm^{3+} quantum efficiency due to the enhanced $^3H_4$ fluorescence lifetime that strongly modifies the local environment of Thulium ions [3]. Observation of Fig. 2 allows for identification of doping levels for a material with desired Δ value; an example is $\Delta = -0.003$, which can be achieved by doping the PCF core with 9 mol% of Al_2O_3 and the PCF cladding with 11 mol% Al_2O_3 [16].

Simulation is performed on different diameters of first ring air-holes, namely d'/Λ from 0.30 to 0.55 in increments of 0.05, and by varying cladding air-holes diameter, d/Λ of 0.25, 0.30, 0.35, and 0.40. As described earlier, the cut-off wavelengths of PCF is determined by the intersection point of effective refractive index of fundamental mode with effective refractive index of cladding mode. Each result of cut-off wavelength for five different values of Δ, from -0.001 until -0.005 with step of 0.001, is plotted in Fig. 3(a)–(e), respectively. Curves on the right hand side indicate the long cut-off wavelength, while those on the left hand side indicate the short cut-off wavelength. The shaded region in Fig. 3(a)–(e) refers to the region where the long and short cut-off wavelength meets the criteria listed earlier in this section. This region is chosen loosely in order to accommodate sufficient tolerance during PCF fabrication. Tolerances in fabrication allow for different values of Δ, d'/Λ, and d/Λ to cause diverse characteristics in resulting PCF, especially regarding the transmission characteristic [15], as shown in Fig. 3(a)–(e). Performance of the PCF band-pass filter is observed to degrade with changes as low as $\pm 1\%$ to the cladding hole-diameter. However, transmission can be maintained above 75 % for tolerances of $\pm 1\%$ on the first ring air-hole diameter. The transmission spectrum is mainly influenced by the number of outer rings, while being independent of fiber length [15]. Furthermore, Fig. 3(c) allows for the observation that the optimized value of $\Delta = -0.003$ gives a higher likelihood of satisfying the band-pass filter criteria. It remains possible to achieve the band-pass filter criteria when fabrications diverge from this optimized value of $\Delta = -0.004$, as can be seen by Fig. 3(d) and (e). Transmission spectra that operates in 1000 nm until 1750 nm regions is found as best achieved by choosing $d/\Lambda = 0.30$ and $d'/\Lambda = 0.35$ at fixed $\Lambda = 3.2$ μm and $\Delta = -0.004$.

Transmission characteristic are evaluated for the proposed PCF design comprising eight rings of air-holes, as [11] predicts that using eight or more rings of air-holes will achieve transmission over 80%. Fig. 4 shows the results of transmission spectra taken from FV-FEM [17]. The perfectly matched layer (PML) boundary condition is used for absorbing radiation from the fiber in order to calculate accurate leakage losses. The transmission reflects the fractional power

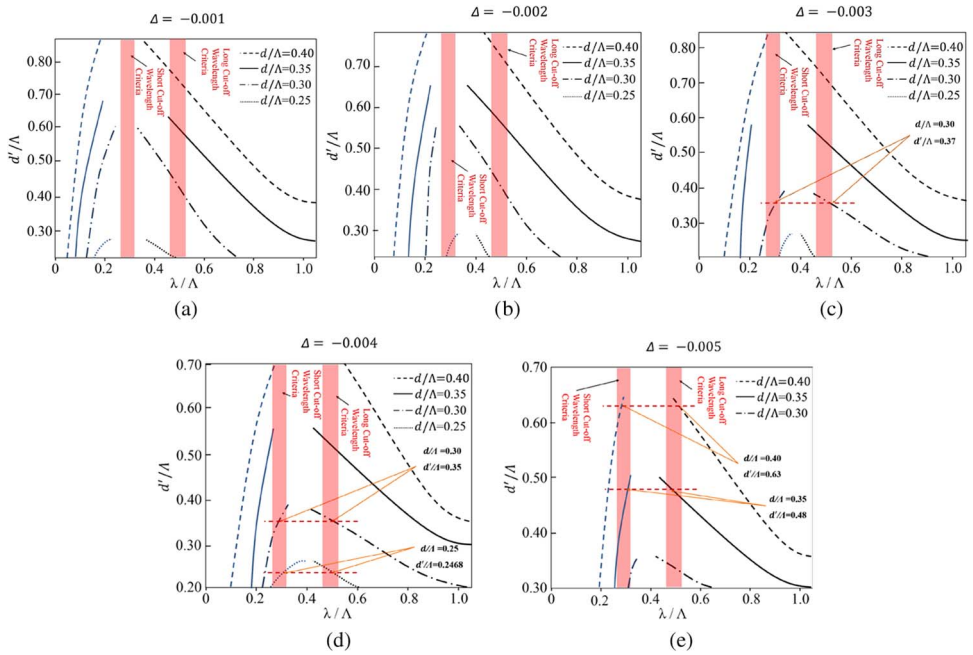

Fig. 3. Long and short cut-off wavelengths as a function of d'/Λ from 0.30 to 0.55 by increment of 0.05 and by varying cladding air-holes diameter d/Λ of 0.25, 0.30, 0.35, and 0.40 for core-cladding doping concentration difference Δ values of (a) −0.001, (b) −0.002, (c) −0.003), (d) −0.004, and (e) −0.005.

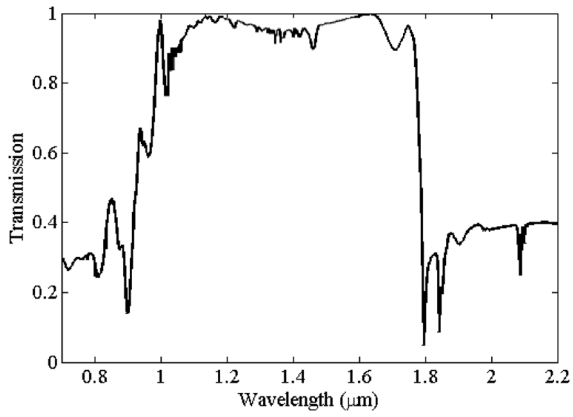

Fig. 4. Modeled transmission spectra.

propagating in the core independently of fiber length. Results reveal that transmission decreases below short cut-off wavelength (800 nm) and above long cut-off wavelength (1750 nm). The highest level of transmission occurs at wavelengths of 1050 nm, 1420 nm, 1470 nm, and 1550 nm.

3. Modeling TD-PCFA

The intended thulium-doped optical fiber preform in this work arises from pure silica tubes fabricated by MCVD and solution doping. This process allows for doping of other materials, such as phosphorus and germanium, to be incorporated in the glass. Solution doping technique is used to dope thulium and aluminum into the glass.

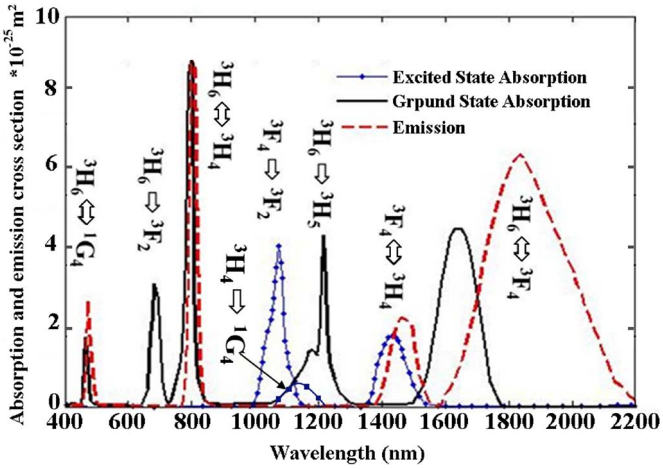

Fig. 5. Emission and absorption spectra of thulium–aluminum co-doped silica fiber.

Fig. 5 indicates the emission and absorption spectra of Tm^{3+}-doped silica fiber at 800 nm, 1400 nm and 1800 nm bands. The spectral emission cross-section at S-band of Thulium ion [18] The emission cross section was measured for three emission bands at 800 nm, 1460 nm, and 1820 nm. These three bands are attributed to the $^3H_6 \rightarrow {}^3H_4$, $^3H_4 \rightarrow {}^3F_4$, and $^3H_6 \rightarrow {}^3F_4$ transitions. The measured emission cross section rate at 800 nm, 1460 nm, and 1820 nm bands are $\sigma_{se} = 3 \times 10^{-25}$ m^2, $\sigma_{se800} = 8 \times 10^{-25}$ m^2, and $\sigma_{se1800} = 5.5 \times 10^{-25}$ m^2. The absorption cross-sections considered in this model closely match the emission cross-sections estimated by the modified McCumber's relation [19]. An inconvenient branching ratio of transitions from $^3H_4$ results in higher emission at 800 nm [20]. Furthermore, the emission at 1800 nm is also significantly higher than at 1400 nm. These results show a stronger ASE at 800 nm and 1800 nm when compared to the intended amplification region at 1400 nm. Suppressing the 800 nm and 1800 nm ASE is thus crucial to allow stronger emission at 1400 nm and corresponding higher S-band amplification. A PCF band-pass filter is introduced in this paper as a means to suppress the 800 nm and 1800 nm ASE.

An existing differential equation-based model [5], [6] that governs transitions between energy levels is updated to include ASE suppression at 800 nm and 1800 nm for S-band gain improvements. Light wave propagation equations along the thulium fiber for 1050 nm pump power (P_P), signal power (P_S), S-band ASE (P_{ase}), 800 nm ASE (P_{ase8}), and 1800 nm ASE (P_{ase18}) in the forward direction $(+)$ and backward $(-)$ direction along the fiber can be established as follows [2]:

$$\frac{dP^{\mp}(\lambda)}{dz} = \Gamma(\lambda)P^{\pm}(\lambda)\sum_{ij}\left(\left(N_i\sigma_{ij}(\lambda) - N_j\sigma_{ji}(\lambda)\right) \pm \Gamma(\lambda)\sum_{ij} 2hv_{ij}\Delta v N_{ii}\sigma_{ij}(\lambda) \pm (\alpha_{P,s})P^{\pm}(\lambda) \quad (1)$$

where α is background scattering loss, which is assumed to be constant for all wavelengths. α_{ASE8} and α_{ASE18} is 800 nm and 1800 nm loss due to PCF bandpass filter. Fig. 6(a) depicts the calculated PCFs propagation loss spectrum from 700 nm to 1800 nm wavelength compared to SMF. This PCF loss was calculated by multiplication of SMF loss with PCFs transmission spectrum, considering loss mechanism in SMF and transmission spectrum of PCF. As expected, there is a significant loss effect on cladding mode, which operates in the wavelength region from 700 nm to 1000 nm compared to that of fundamental mode which operates within 1000 to 1750 nm. Further wavelength also shows that loss increased once again as the propagation operates in cladding mode above the 1750 nm wavelength. The loss

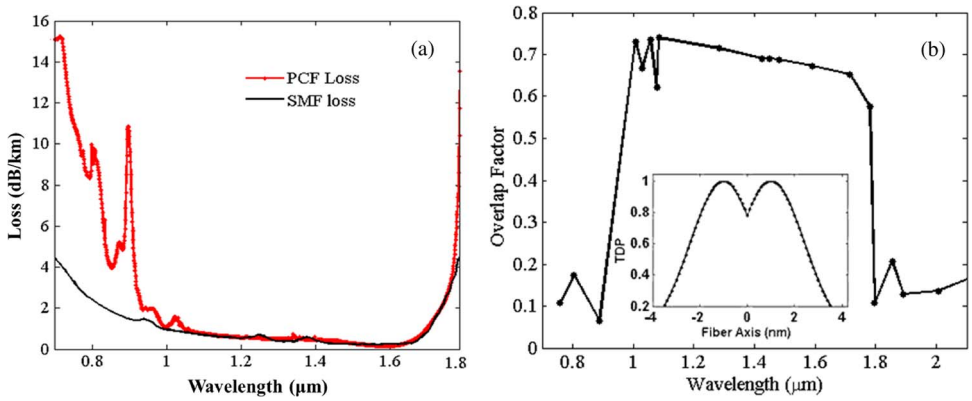

Fig. 6. (a) SMF and proposed PCF loss spectrum, (b) Overlap factor curve for TD-PCFA, with the inset describing a transversal distribution of the optical intensity around the fiber core.

values for 800 nm, 1800 nm, and 1400 nm S-band region are added with background loss in the light wave propagation equations to simulate gain and noise figure.

Overlap factor $\Gamma(\lambda)$ is a measure of the optical mode fraction overlapping with the doped ions at the central core distribution, wherein absorption or emission stimulation occurs via rare earth ion transitions. This overlap factor can be calculated based on the electric field distribution for a particular fiber as follows [19]:

$$\Gamma(\lambda) = \frac{2\pi \int_0^{\infty} |E(r,\varphi,\lambda)|^2 \times n_T(r) \times r \times dr}{N_T \int_0^{\infty} |E(r,\varphi,\lambda)|^2 \times r \times dr}. \tag{2}$$

In this equation, $E(r,\varphi,\lambda)$ refers to the guided mode's electric field, while N_T is the total doping concentration of thulium ions per unit length, and $n_T(r)$ represents the transverse distribution profile (TDP) of the TD-PCFA [21], [22].

The FV-FEM technique is utilized in order to calculate the electric field in the PCF fiber. Fig. 6(b) contains a typical curve of $\Gamma(\lambda)$ TD-PCFAs with optimized D of 3.2 μm, d'/Λ of 0.35, d/Λ of 0.30, and $\Delta = -0.004$. Overlap is very low between optical modes below λ_S and dopant ions in PCF, which can be expected from the electric field intensity analysis provided in Fig. 7. Where the cladding mode takes place in this wavelength region with the field radiating inside the cladding instead of central core, and this behavior occurs when the cladding effective index is higher than the fundamental mode effective index. Wavelengths in excess of λ_S, cause the overlap factor to increase sharply. This observation is a result of the electric field starting to operate in guided mode at the central core, whereupon a high portion of the optical mode overlaps with doping ions as can be clearly seen in Fig. 7(b)–(e). As wavelength increases past the long cut-off wavelength threshold, the electric field once again propagates inside the cladding region as illustrated in Fig. 7(f). Hence, the overlap factor is strongly reduced for operating wavelength in excess of this cut-off threshold.

4. Results and Discussion

Observed 800 and 1800 nm ASE bands are reported to affect the S-band total gain in TDFAs [7], [10]. Within this current work, Fig. 8(a) and (b) provide a comparison between normal TDFA and TD-PCFA as a function of position on stimulated forward and backward travelling of both 800 nm and 1800 nm ASE power. A fixed pump power of 1050 nm at 350 mW employed inside the numerical model will cause a suppression of both 800 nm and 1800 nm in the TD-PCFA and consequent increase in ASE at the 1400 nm band (see Fig. 8(c)). This result can be explained by the inclusion of TD-PCFA effectively decreasing an ion population in the ground state $^3H_6$ whilst assisting population of the ion at $^3F_4$ energy level, thus allowing 1050 nm light to

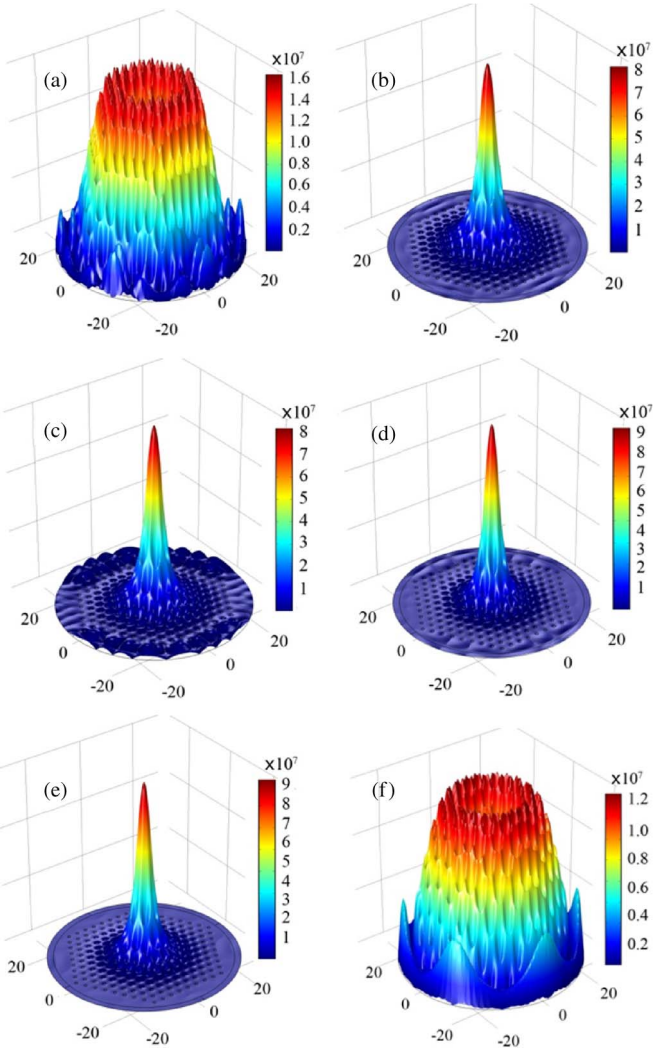

Fig. 7. Electric field distribution at pump power wavelength (a) 800 nm, (b) 1000 nm, (c) 1050 nm, and signal wavelength (d)1460 nm, (e) 1700 nm, and (f) 1800 nm.

efficiently excite the ion to the higher level, $^3H_4$. The latter effect reduces the fractional inversion at different longitudinal positions of the fiber at a shorter distance. Lower fractional inversion results in an increase of population inversion between the $^3F_4$ and $^3H_4$ level and, consequently, increases the stimulated emission in the S-band region [23].

Results of gain on both normal TDFA and TD-PCFA, as depicted in Fig. 8(d), is calculated by fixing input signal wavelength at 1460 nm and input power as −30 dBm, while 1050 nm pump power is fixed at 350 mW. As observed from comparison between both gains medium, normal TDFA saturates at 15 m fiber length, which can be considered as an optimized length.

Higher signal and pump overlap factor in the TD-PCFA in contrast to normal TDFA will cause a greater amount of pump power to be depleted, and result in optimized fiber length decreasing to 11 m. This phenomenon is also observable in 1460 nm ASE situations.

Fig. 9 shows variation of the gain and noise figures across the input signal wavelength for the normal TDFA and TD-PCFA. The input signal and 1050 nm pump powers are fixed at −30 dBm and 350 mW respectively. Optimized length for the normal TDFA and TD-PCFA is fixed at 15 m and 11 m respectively. As shown in the figure, gain enhancements of about 4.5 dB are obtained using TD-PCFA at a wavelength region between 1450 and 1470 nm. This enhancement is

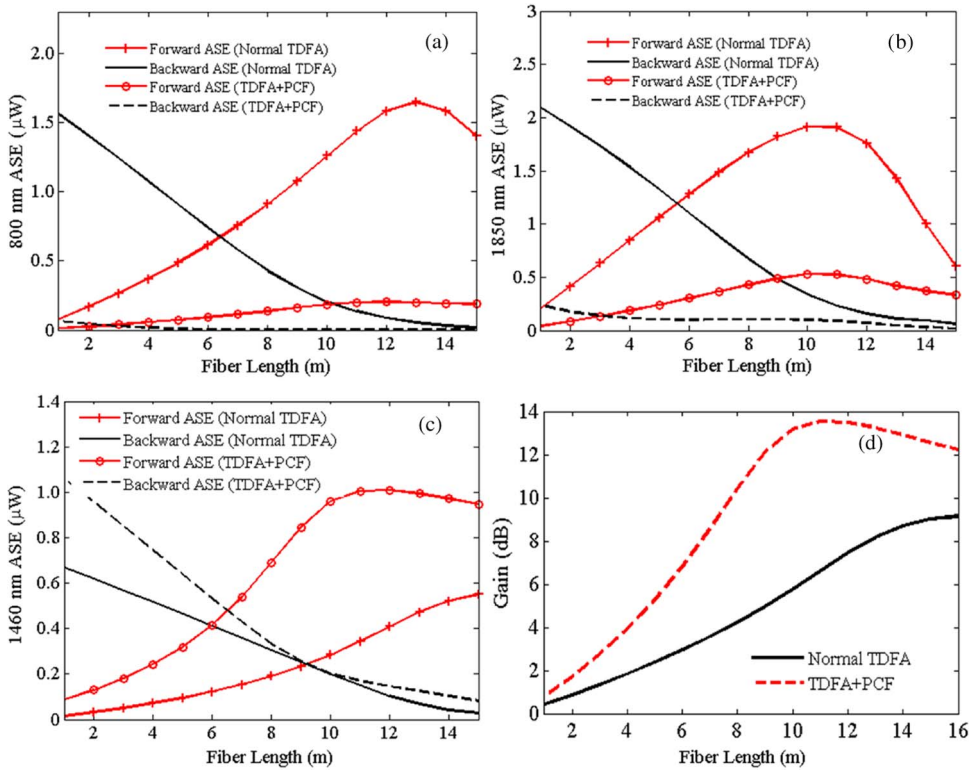

Fig. 8. (a)–(c) Forward and backward travelling ASE for normal TDFA and TD-PCFA as a function of position in the TDF at (a) 800 nm, (b) 1800 nm, (c) 1460 nm, and (d) gain as a function of position in the normal TDFA and TD-PCFA.

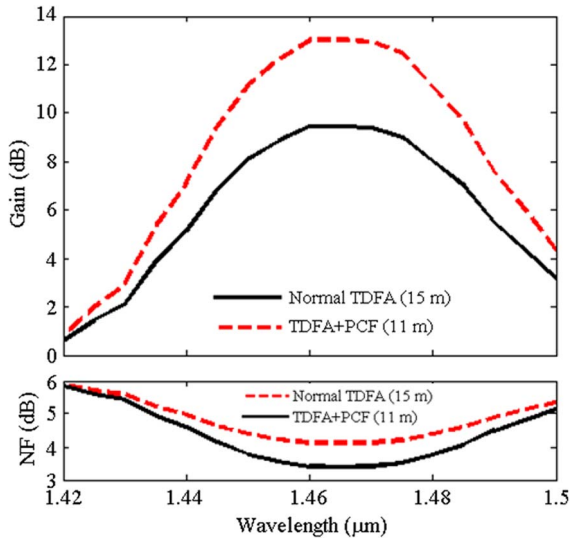

Fig. 9. Gain spectrum for normal TDFA with optimized length of 15 m and TD-PCFA with optimized length of 11 m.

attributed to ASE suppression at 800 and 1800 nm. Furthermore, the noise figure is also observed from Fig. 9 to be improved by about 1–3 dB with the TD-PCFA, whereby the increased gain has a consequent impact on the noise figure, as described in the standard noise figure equation [19].

5. Conclusion

The optimized design of TD-PCFA is shown numerically. A recommendation for TDFA design is for wavelengths above 1000 nm to propagate with low loss and high overlap factor in order to maximize the efficiency of 1050 nm pumping. Thulium absorption overlap factor is adjusted through PCF to allow the fundamental mode of the S-band signal to propagate with minimum loss and high overlap factor. Meanwhile, the 800 nm and 1800 nm ASE encounters higher loss and low overlap factor. The optimized PCF geometrical structure is found at $\Lambda = 3.2$ μm, $d'/\Lambda = 0.35$, $d/\Lambda = 0.30$, and $\Delta = -0.004$ in the course of achieving the above criteria. The performance was also evaluated against fabrication tolerance for practical consideration. This PCF-TDFA approach improves the gain of TDFA by 5 dB in the S-band region, which represents a promising foundation for subsequent research efforts.

Acknowledgement

The authors wish to acknowledge the valuable discussions and support from P. Peterka and P. Koska of the Institute of Photonics and Electronics, Prague, Czech Republic.

References

[1] P. R. Watekar, S. Ju, and W. T. Han, "A small-signal power model for Tm-doped silica-glass optical fiber amplifier," *IEEE Photon. Technol. Lett.*, vol. 18, no. 19, pp. 2035–2037, Sep./Oct. 2006.
[2] B. Faure, W. Blanc, B. Dussardier, and G. Monnom, "Improvement of the Tm3+:(3) H-4 level lifetime in silica optical fibers by lowering the local phonon energy," *J. Non-Crystalline Solids*, vol. 353, pp. 2767–2773, Sep. 15, 2007.
[3] B. Faure, W. Blanc, B. Dussardier, G. Monnom, and P. Peterka, "Thulium-doped silica-fiber based S-band amplifier with increased efficiency by aluminum co-doping," *Opti. Amplifiers Appl.*, San Francisco, CA, USA, 2004, p. OWC2.
[4] P. Peterka, B. Faure, W. Blanc, M. Karasek, and B. Dussardier, "Theoretical modelling of S-band thulium-doped silica fibre amplifiers," *Opt. Quantum Electron.*, vol. 36, no. 1–3, pp. 201–212, Jan./Feb. 2004.
[5] S. D. Emami *et al.*, "New design of a thulium–aluminum-doped fiber amplifier based on macro-bending approach," *J. Lightw. Technol.*, vol. 30, no. 20, pp. 3263–3272, Oct. 15, 2012.
[6] S. D. Emami *et al.*, "Micro-bending based optical band-pass filter and its application in S-band Thulium-doped fiber amplifier," *Opt Exp.*, vol. 20, no. 28, pp. 29 784–29 797, Dec. 31, 2012.
[7] S. K. Varshney, K. Saitoh, M. Koshiba, B. P. Pal, and R. K. Sinha, "Design of S-band erbium-doped concentric dual-core photonic crystal fiber amplifiers with ASE suppression," *J. Lightw. Technol.*, vol. 27, no. 11, pp. 1725–1733, Jun. 1, 2009.
[8] F. Poli, M. Foroni, A. Cucinotta, S. Selleri, and P. Vavassori, "Single-stage S-band depressed-cladding EDFA with bending loss ASE suppression," presented at the Eur. Conf. Opt. Commun., Glasgow, U.K., 2005, Paper TH3.3.6.
[9] K. G. Hougaard and K. G. Hougaard, "*Rare-Earth Doped Photonic Crystal Fibre Lasers and Amplifiers*," Ph.D. dissertation, Tech. Univ. Denmark, Kgs. Lyngby, Denmark, 2005.
[10] L. Labonte *et al.*, "Design, computation and characterization of Thulium-doped photonic crystal fibre for emission around 1700 nm," *Proc. ICTON*, 2009, vol. 1/2, pp. 950–953.
[11] S. K. Varshney *et al.*, "Strategies for realizing photonic crystal fiber bandpass filters," *Opt Exp.*, vol. 16, no. 13, pp. 9459–9467, Jun. 23, 2008.
[12] S. D. Emami, A. R. Muhammad, S. W. Harun, H. Ahmad, and H. A. Abdul Rashid, "S-band thulium-doped fiber amplifier enhancement using ASE suppression" in *Proc. Opt. Fiber Commun. Conf.*, 2014, pp. 1–3.
[13] F. Poli, A. Cucinotta, and S. Selleri, "Photonic crystal fibers properties and applications," in *Materials Science*, vol. 102. Dordrecht, The Netherlands: Springer-Verlag, 2007.
[14] P. S. J. Russell, "Photonic-crystal fibers," *J. Lightw. Technol.*, vol. 24, pp. 4729–4749, Dec. 1, 2006.
[15] S. K. Varshney, M. P. Singh, and R. K. Sinha, "Propagation characteristics of photonic crystal fibers," *J. Opt. Commun. (Germany)*, vol. 24, no. 5, pp. 192–198, May 5, 2003.
[16] W. M. Haynes, *CRC Handbook of Chemistry and Physics*, 94th ed. Boca Raton, FL, USA: CRC, 2011.
[17] F. Fogli, L. Saccomandi, P. Bassi, G. Bellanca, and S. Trillo, "Full vectorial BPM modeling of index-guiding photonic crystal fibers and couplers," *Opt. Exp.*, vol. 10, no. 1, pp. 54–59, Jan. 14, 2002.
[18] J. Michael and F. Digonnet, *Rare-Earth-Doped Fiber Lasers and Amplifiers*. Boca Raton, FL, USA: CRC, 2001.
[19] E. Desurvire, *Erbium-Doped Fiber Amplifiers: Principles and Applications*. New York, NY, USA: Wiley, 1994.
[20] T. Sakamoto, S. Aozasa, M. Yamada, and M. Shimizu, "Hybrid fiber amplifiers consisting of cascaded TDFA and EDFA for WDM signals," *J. Lightw. Technol.*, vol. 24, no. 6, pp. 2287–2295, Jun. 2006.
[21] J. C. Martin, "Erbium transversal distribution influence on the effectiveness of a doped fiber: Optimization of its performance," *Opt. Commun.*, vol. 194, no. 4–6, pp. 331–339, Jul. 15, 2001.
[22] S. D. Emami, H. A. Abdul-Rashid, H. Ahmad, A. Ahmadi, and S. W. Harun, "Effect of transverse distribution profile of thulium on the performance of thulium-doped fibre amplifiers," *Ukrainian J. Phys. Opt.*, vol. 13, no. 2, pp. 74–81, 2012.
[23] T. Kasamatsu, Y. Yano, and T. Ono, "1.49-Km-band gain-shifted thulium-doped fiber amplifier for WDM transmission systems," *J. Lightw. Technol.*, vol. 20, no. 10, pp. 1826–1838, Oct. 2002.